HardwareX 16 (2023) e00485

Contents lists available at ScienceDirect

HardwareX

journal homepage: www.elsevier.com/locate/ohx

Development of an Inertial Measurement Unit (IMU) with datalogger and geopositioning for mapping the Earth's magnetic field

J.S. Botero-Valencia [a,*], M. Mejía-Herrera [a], D. Betancur-Vásquez [b]

[a] Grupo de Sistemas de Control y Robótica (GSCR), Instituto Tecnológico Metropolitano, Medellín, Colombia
[b] Grupo de Investigación en Tecnologías Emergentes Sostenibles e Inteligentes (GITESI), Institución Universitaria de Envigado, Medellín, Colombia

ARTICLE INFO

Keywords:
Datalogger
Earth magnetic field
Geopositioning
Inertial Measurement Unit
Magnetometer

ABSTRACT

The Earth's magnetic field is used in various navigation systems, but this field has a dynamic behavior that can be affected by different physical factors in local environments. These factors can pose risks to navigation systems and at the same time be a signal of a phenomenon that needs to be investigated, such as mineral concentration or the presence of interference from electrical equipment, among others. For that reason, in this project, this system was designed and integrated using a low-cost, military-grade magnet inductive magnetometer, which is integrated into two Inertial Measurement Units to corroborate the movement data, and at the same time a geopositioning system to georeference the sensor measurements. The information is managed by an MCU, which also stores data on an SD card. The system includes a lithium battery management system to provide more than an hour of autonomy. Wireless communication systems are intentionally avoided to prevent interference, and an infrared transmission LED is included instead, in case the real-time transmission is necessary. The results show that the proposed system allows for obtaining maps of magnetic field intensity in open spaces, and this information can be used to determine regions with anomalies.

Specifications table	
Hardware name	
Subject area	• Engineering • Instrumentation
Hardware type	• Measuring physical properties and in-lab sensors • Field measurements and sensors • Electrical engineering and computer science
Open source license	Creative Commons Attribution-ShareAlike license
Cost of hardware	USD 255.79
Source file repository	https://doi.org/10.17605/OSF.IO/WXHYM

1. Hardware in context

The Earth's magnetic field is an invisible but very important force that surrounds the Earth and extends out into space. This force is generated in the Earth's inner core, which is a molten metal ball containing iron and nickel. The importance of the Earth's

* Corresponding author.
E-mail address: juanbotero@itm.edu.co (J.S. Botero-Valencia).

https://doi.org/10.1016/j.ohx.2023.e00485
Received 11 March 2023; Received in revised form 16 September 2023; Accepted 26 October 2023
2468-0672/© 2023 The Author(s). Published by Elsevier Ltd. This is an open access article under the CC BY-NC-ND license (http://creativecommons.org/licenses/by-nc-nd/4.0/).

magnetic field is that it acts as a kind of protective shield for the Earth. It protects our planet from solar winds and other charged particles coming from the Sun. In addition to protecting the Earth from cosmic radiation, the magnetic field is also important for navigation. Compasses work thanks to the Earth's magnetic field, as the north pole of a compass is oriented towards the Earth's magnetic south pole and special concentrations of minerals or other materials can also be associated with the deformation of the same. In short, the Earth's magnetic field is important because it acts as a protective shield for the Earth, protecting us from charged particles from the Sun and enabling compass navigation.

The progress of research in microelectronics and electromagnetic materials (MEMS) for sensors has allowed the design and development of devices for everyday use for the detection of patterns in natural phenomena [1]. The integration of MEMS sensors such as accelerometers, magnetometers, and gyroscopes (IMU) enables complete measurement of an object's state of inertia and the magnetic field's state, indicating its position on the axis orthogonal to the earth's surface [2]. While sensors that measure magnetic fields are often utilized for other variables such as current and orientation (such as Hall and Z orientation sensors) in different fields such as welding mechanics [3], medicine [4,5], robotics [6], among others [7]. The implementation of Hall effect sensors for magnetic measurement can present challenges in uncontrolled environments due to specific positioning and measurement requirements [7]. As a result, researchers seek alternative methods to measure magnetic fields, expanding the use of these sensors to detect fields and anomalies in less accessible areas [8]. Selecting the ideal sensor for a specific application requires considering factors such as sensitivity, linearity, range, and maximum sampling frequency [9]. The sensing model is determined by the material of the sensor, the axis in which it measures a 3D field, and its different gradients. Magnetic fields have an advantage in their ability to easily pass through various materials, making them favorable over other measurement sensors such as acoustic, electrical, or mechanical sensors [10]. The feasibility of implementing electronic sensory devices in hostile environments requires hermetic protection, enabling the measurement of magnetic fields between conductive and non-conductive materials of electrical energy.

This paper presents a magnetometer device supported by three inertial measurement units that offer different values of magnetic field for data correction or hardware failure detection, battery charging system, and GPS for geolocating the gathered data. The system implements I2C communication and modular sensors that can be easily connected to any other centralized data device, allowing for their simple deployment at a commercial level [11]. The device is small in size, and easy to transport, and use. Its ability to geolocate and detect magnetic field changes makes it a fast and practical way of identifying anomalies and creating magnetic field maps, both in open and closed environments [12], And due to the importance of the magnetometer calibration process [13–15], a least-squares regression alignment of the axes was performed using the acquired data. For guarantee that the magnetic field measurements taken by the magnetometer are accurate.

2. Hardware description

The proposed device is a low-cost magnetometer that is geo-positioned and equipped with two Inertial Measurement Units (IMU) or absolute position sensors of nine degrees-of-freedom (DOF), GPS, an infrared transmitter for data transmission without affecting the magnetic field of the device, a rechargeable one-cell Li-Po battery, and a military-grade magnetometer suitable for military and aerospace applications, such as those referenced in [16]. It can measure magnetic fields with an accuracy of up to 50 nT, comparable to the magneto accuracy of the Casimir satellite, which has an accuracy of 40 nT [17].

The system was designed using computer-aided design (CAD) and built using additive manufacturing (AM) technology to facilitate future customization if necessary. All design files, including the bill of materials, can be found at the link and are subject to the following open hardware licenses: CC BY 4.0.

The system was designed to withstand underwater conditions and was tested for ground truth measurement acquisition in a pool at a depth of 1.5 meters. However, the system's ingress protection level has not been determined yet. The proposed system consists of a stack of sensors, as shown in Fig. 1, inside a 2-inch PVC pipe, sealed with a welded cap on one side and a threaded cap on the other side for easy access to turn on/off the system and remove the SD card.

- The proposed system is designed to be portable, allowing for data acquisition on robotic platforms for remote exploration and mapping of magnetic field changes associated with various phenomena such as metal deposits, communications, navigation, or submarine detection.
- The system is low-cost and user-friendly, and its construction allows for easy integration into more complex systems, thereby enhancing research possibilities in the analysis of magnetic fields and enabling the deployment of sensor mesh to analyze changes in the magnetic field covering larger geographic areas.
- If the measurement is taken in an open space, the acquired data is georeferenced using location data, to link the measurements to a specific location on the Earth's surface. Georeferencing enables the construction of maps or contour plots that accurately represent the spatial distribution of magnetic field measurements. These maps or contour plots can be used to observe and analyze deformations or variations in the magnetic field over a geographic area, such as in geological surveys or environmental monitoring.
- It is a flexible system that uses free and open-source software (FOSS), enabling integration with other systems. Additionally, IMU measurements are acquired from different sensors to reduce failures and validate possible data or hardware errors.
- The system does not count on wireless communication but IR communication to protect the quality of the measurements, which would be stored in the SD, or transmitted via IR.

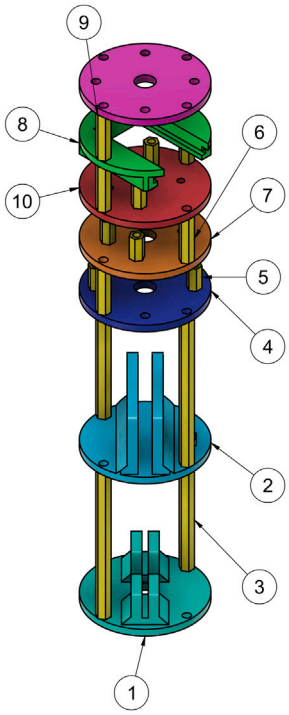

Parts List		
Item	Qty	Part Number
1	1	BaseGPS
2	1	BaseBattery
3	4	Brass Separator H-H M3x65mm
4	2	BaseSEN14001[RazorIMU]
5	6	Brass Separator H-H M3x10mm
6	6	Brass Separator H-H M3x20mm
7	1	BaseDFR0095[IR]
8	1	BaseRM3100
9	2	Brass Separator H-M M3x20x6mm
10	1	Base4646[BNO055]

Fig. 1. The mechanical structure and table of materials of the system are documented, with numbered annotations on the image corresponding to each part in the table. The name of each part contains the reference of the device it holds, enabling easy identification of each device's location within the system.

3. Design files

This section details the files necessary to replicate the proposed device. It is important to note that the structure is modular, allowing for the exclusion of certain sensors. The parts to be printed are available in STEP format to allow editing or in STL to facilitate printing directly.

3.1. Design files summary

Design filename	File type	Open source license	Location of the file
Base4646[BNO055]	STL	CC-BY-4.0	https://osf.io/qxayk
BaseBattery	STL	CC-BY-4.0	https://osf.io/bzqhe
BaseDFR0095[IR]	STL	CC-BY-4.0	https://osf.io/wxu7r
BaseGPS	STL	CC-BY-4.0	https://osf.io/e69qm
BaseRM3100	STL	CC-BY-4.0	https://osf.io/sd2hf
BaseSEN0253[BNO055]	STL	CC-BY-4.0	https://osf.io/qyteb
BaseSEN14001[RazorIMU]	STL	CC-BY-4.0	https://osf.io/jpfz8
Base4646[BNO055]	STEP	CC-BY-4.0	https://osf.io/znc32
BaseBattery	STEP	CC-BY-4.0	https://osf.io/jkzqn
BaseDFR0095[IR]	STEP	CC-BY-4.0	https://osf.io/d7phc
BaseGPS	STEP	CC-BY-4.0	https://osf.io/yjz63
BaseRM3100	STEP	CC-BY-4.0	https://osf.io/v6tb4
BaseSEN0253[BNO055]	STEP	CC-BY-4.0	https://osf.io/uwqdz
BaseSEN14001[RazorIMU]	STEP	CC-BY-4.0	https://osf.io/86eb2
RM3_MPU_BNO_GPS.ino	ino	CC-BY-4.0	https://osf.io/m5b2f

4. Bill of materials

This section presents all the hardware involved in system construction, prices, quantities, references, and sources of materials for replicating the proposed device.

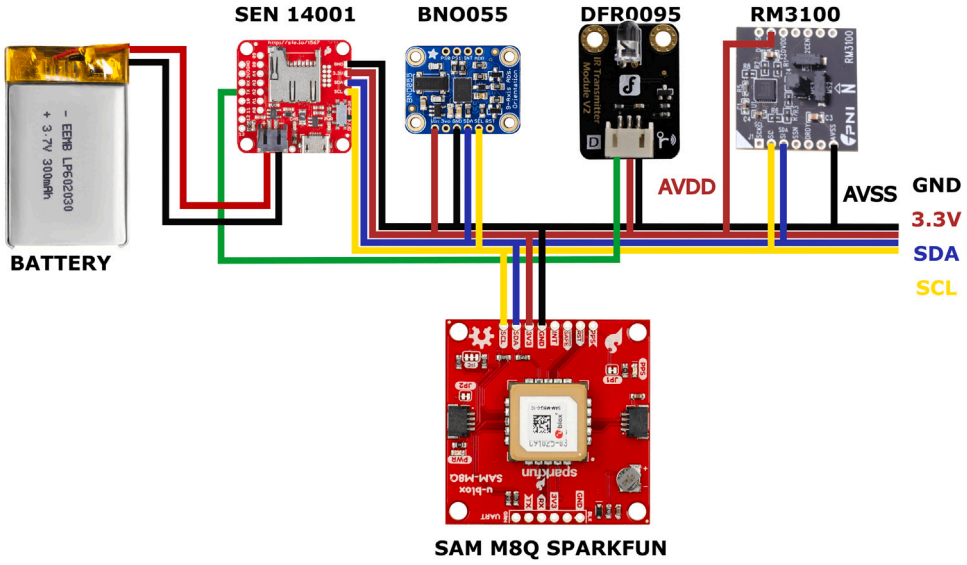

Fig. 2. Schematic connections of the designed system.

Designator	Component	Amount	Cost per unit USD	Total cost USD	Source of materials	Material type
14190	RM3100	1	25.00	25.00	Link	-Composite
4646	BNO055	1	29.95	29.95	Link	-Composite
SEN14001	MCU	1	48.00	48.00	Link	-Composite
DFR0095	IR Transmitter	1	3.90	3.90	Link	-Composite
DFR0094	IR Receiver	1	3.90	3.90	Link	-Composite
GPS15210	GPS	1	42.95	42.95	Link	-Composite
M3 hardware	M3 Assortment Kit	1	16.99	16.99	Link	-Structural
M3 hardware	Postes M3	1	8.49	8.49	Link	-Structural
PLA	PLA	1	18.99	18.99	Link	-Structural
2″ PVC	PVC Pipe	1	23.06	23.06	Link	-Structural
2″ PVC	PVC Welded cap	1	11.77	11.77	Link	-Structural
2″ PVC	PVC Screw cap	1	9.99	9.99	Link	-Structural
2″ PVC	PVC Male adapter	1	12.80	12.80	Link	-Structural
				255.79		

5. Build instructions

The Design files table lists all the items available in STL format that require 3D printing or other 3D manufacturing technology for production. After printing each design, you must take each part and fix the respective sensor using 10 mm M3 spacers. For instance, the DFR0095 sensor requires fixing to the BaseDFR0095 part. Once you have fixed each sensor to each base, follow the schematic of the Fig. 2 to make the necessary connections.

Please note that all printed parts, except for the BaseBattery, have a central perforation that enables system cables to pass through without interfering with the PVC enclosure. For the sensor tower, use M3 separators following the design presented in Fig. 1. It is possible to change the order of hardware as desired or add new elements by modifying the existing STL files since the system uses an I2C bus that allows up to 1024 devices. To complete the system is necessary to create the enclosure or housing. To start take a 2-inch diameter PVC pipe and cut a 60 cm length. Then, use PVC pipe glue to fix the screw-less plug to one end of the tube and the male adapter for the PVC pipe to the other end. After the glue dries completely, insert the sensor stack into the tube, and close the housing using the screw cap. The final product should resemble the one presented in Fig. 3. If the system moves inside the housing, we recommend adding a piece of foam to correct this situation.

6. Operation instructions

As previously stated, the system comprises a single-cell lipo-type battery that is linked to the SEN-14001. The SEN-14001 stores data from the other sensors and regulates the battery's charge. The system's operation is straightforward. To access the electronics of the system, the threaded cap at one end of the system must be removed. After taking off the threaded cap and the internal cap,

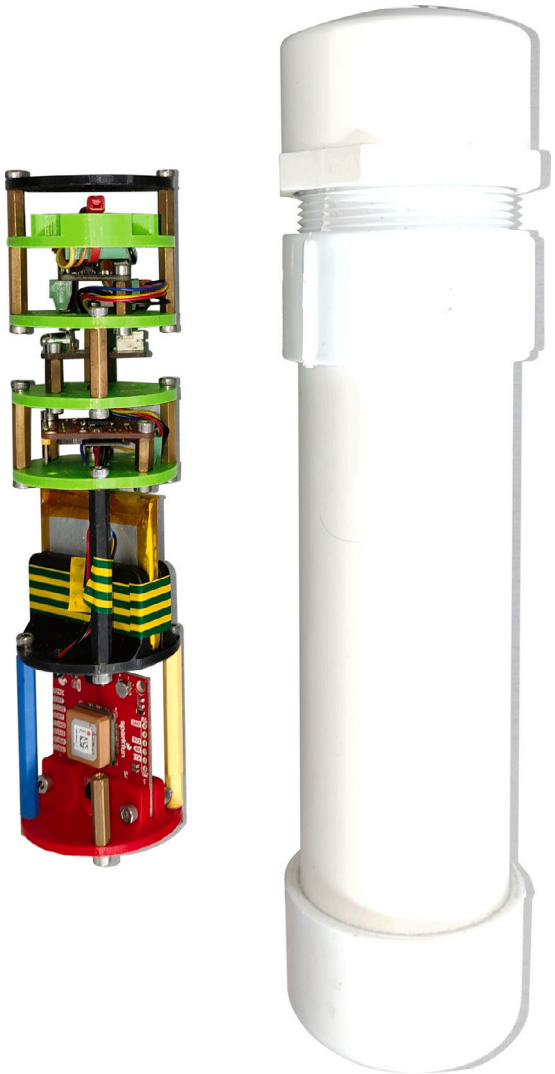

Fig. 3. Real system assembly, the stack of sensors, and the PVC enclosure.

the sensor stack should be removed, and the SEN-14001 sensor, located at item 4 of Fig. 1, must be retrieved. This card contains a power switch, displayed in Fig. 4.

Turn the switch to the power position. If the battery is charged, a red LED will light up, indicating that the system is powered on. If the battery requires charging, connect the SEN14001 to a 5v source using a Micro-USB cable. After the system is energized, it will automatically begin collecting and storing data. Then, put the system back inside the PVC pipe, insert the internal plug, and seal the system by threading the outer cap. To ensure the proper operation of the GPS, it is recommended to take the system outside and wait a few minutes to locate satellites and fix the location.

At the end of the data collection, remove the plugs again, switch the power off, and remove the SD card to extract the data. The data is divided into 8 files, and the contents of each file are listed in the following Table 1.

Each file is a comma-separated values file in which the first column corresponds to the time relative to the device's startup.

6.1. Data processing

The data acquired by Inertial Measurement Units (IMUs) have inherent noise due to their manufacturing process, and in most cases, require data processing to obtain derived information from them. For this reason, in this subsection, we present a proposed methodology for deriving the gravity vector and changes in the magnitude of the magnetic field independently of the orientation of the acquisition system proposed and developed in this work.

Since the internal construction of each sensor and its relative positioning within the system reflect differences in the measurements, an alignment stage was performed, as shown in 5. Initially, since the information acquisition process was developed on a

Table 1
SD Content after data gathering.

File name	Content
BNOA	BNO055 Accelerometer information
BNOG	BNO055 Gyroscope information
BNOM	BNO055 Magnetometer information
GPS	Geolocation information delivered by the M8Q SAM
MPUA	MPU 9250 Accelerometer information
MPUG	MPU 9250 Gyroscope information
MPUM	MPU 9250 Magnetometer information
RM3100	RM3100 Magnetometer information

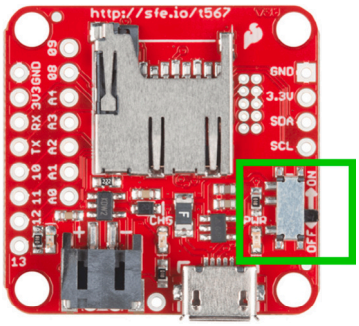

Fig. 4. System power switch location.

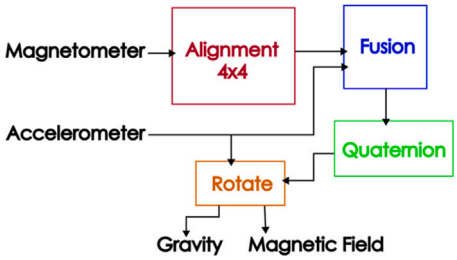

Fig. 5. Magnetometer/Accelerometer calibration and axes alignment process.

single card and the SD card writing process was not instantaneous, there were short time delays between the measurements obtained, so to acquire the measurements with the same time stamps, data interpolation was performed. The alignment block receives the magnetic field data from the trajectories performed for validation using the robotic arm and calculates a 4×4 matrix through least squares regression using the RM3100 as a reference. This calculation helps to correct the information obtained by the MPU and the BNO sensors, to contain the same scale and axes alignment.

After the alignment stage, the information goes to a fusion stage that is responsible for obtaining the absolute orientation of the system using the information from the aligned magnetometers and the accelerometer data. This information is calculated as a quaternion and is used to correct the local orientation of the raw accelerometer data and the aligned magnetometer data. Such calibration allows the system to obtain the real magnitudes of the magnetic fields for each sensor. In the case of gravity, the direction of the field is opposite to the ground, while for the magnetic field, measurements appear as if the system were static, thanks to the quaternion orientation correction.

7. Validation and characterization

Initially, to validate and align the 3 Inertial Measurement Units, the complete system was installed on the last degree of freedom of a KUKA KR5 arc HW industrial robot. The purpose of using this industrial robot is that the positioning accuracy reaches 0.04 mm, and generates controlled movements by rotating the prototype proposed in this article in the YZ plane as seen in Fig. 6(b), in the XY plane in Fig. 6(c), and in XZ in Fig. 6(a). For each position (P1, P2, P3) rotation movements are performed every 4°, that is 90 steps in a complete turn, system sampling time is 1 second, the robot stops 4 seconds at each position, the full data were stored and used to adjust the offset and scale in the axes. The method is similar to that presented in [18], where it was used to calibrate an IMU.

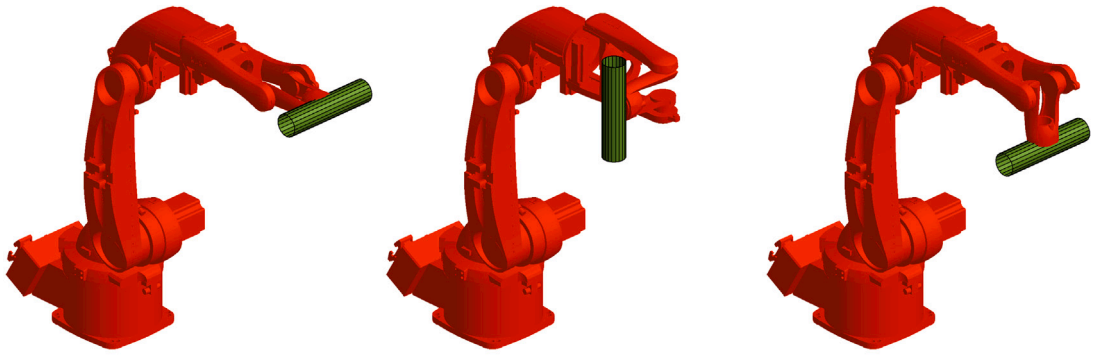

(a) P1 (b) P2 (c) P3

Fig. 6. Robot acquisition positions.

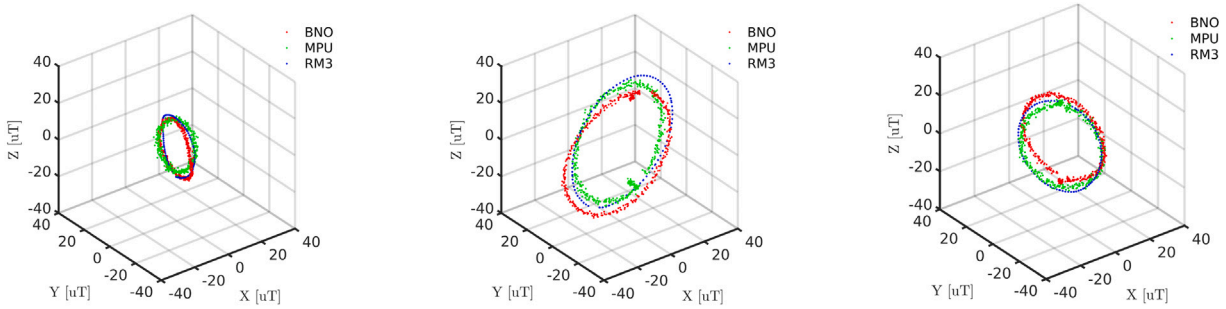

(a) P1 (b) P2 (c) P3

Fig. 7. Magnetometer data.

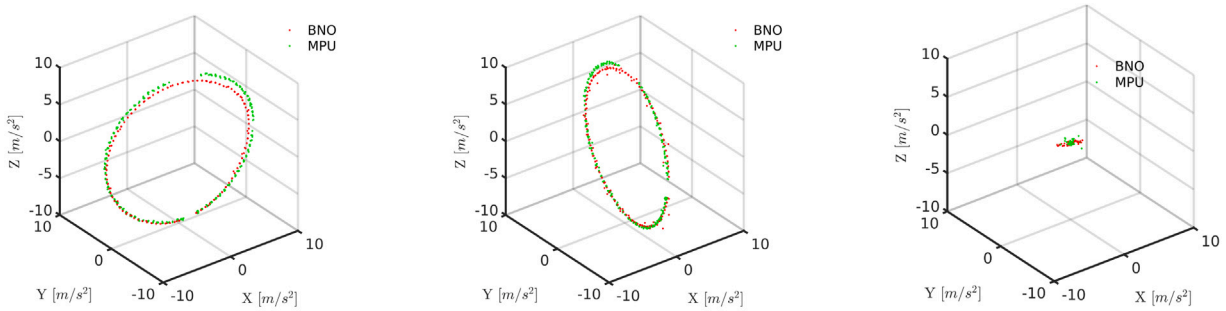

(a) P1 (b) P2 (c) P3

Fig. 8. Accelerometer data.

Fig. 7 shows the change in the magnetic field during the performed test, where only the center was adjusted by removing the mean. The figure highlights the data obtained from three different magnetometers, with the RM3100 magnetometer data appearing much smoother in all three cases. However, while there are differences in the smoothness of the data, the shape and scale of the trajectory for all three magnetometers are similar, suggesting that the overall performance of the three sensors is comparable. The results presented in Figs. 7(a), 7(b), and 7(c) correspond to the positions of the robot in Fig. 6.

Fig. 8 shows the path taken by the accelerometers for each movement of the system. It is worth noting that the RM3100 is limited to measuring magnetic fields, while the BNO055 and MPU9250 are complete inertial measurement units that include an accelerometer, magnetometer, and gyroscope. Any changes in movement measured at each position are due to the alteration of the angle of gravity, which is perpendicular to the ground in this instance. Fig. 8(c) demonstrates minimal changes in movement, as the Z-axis moves parallel to the ground plane.

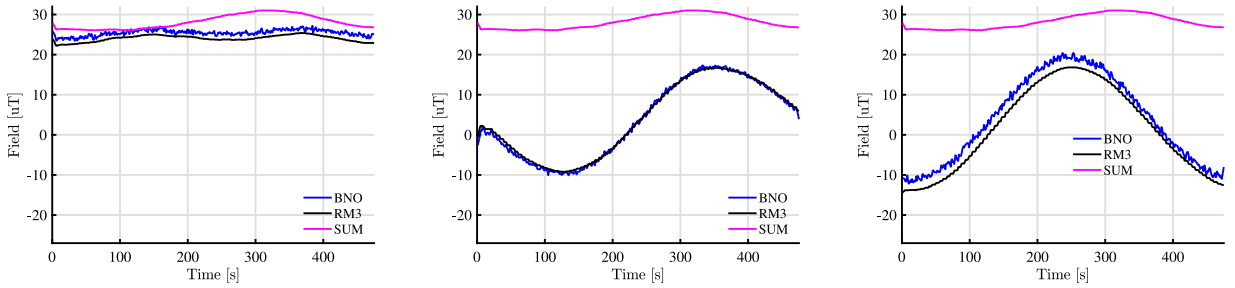

(a) X (b) Y (c) Z

Fig. 9. Magnetometer data.

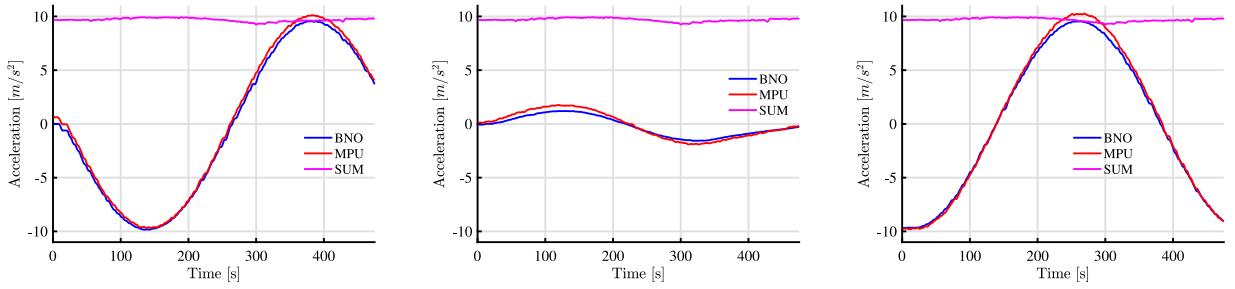

(a) X (b) Y (c) Z

Fig. 10. Accelerometer data.

7.1. Data processing

Fig. 9 shows the magnetic field measurement of the BNO055 magnetometer after applying the alignment matrix obtained by least squares, where the reference was the measurement of the RM3100 magnetometer, which, as mentioned and can be seen in the datasheet, is of better quality. It is observable that the error decreased from 15% to 1% after alignment.

The data acquired during the validation is presented in this section. In Fig. 9, the SUM line represents the sum of the magnitude of the magnetic field, also taken as verification. Due to that alignment problems can occur when the physical installation of sensors does not correspond to the axes of each other. For example, when the Y axis of one sensor may be the X axis of another. This can be corrected with the previously defined 4×4 matrix, without losing the functionality of the rest of the magnetometers.

Along the same lines and to show that the axes of the accelerometers correspond, Fig. 10 compares the two sensors that have an accelerometer, as well as the total SUM as a verification measurement. The acquisition algorithm presented in this paper uses the MPU9250 accelerometer, which has a default scale of 16384 LSB/g. This means that each LSB (least significant bit) of the accelerometer data represents an acceleration of 1/16384 g. However, to convert the accelerometer data to $\mathrm{m/s^2}$, the scale must be multiplied by 10. Because 1 g is equal to 9.80665 $\mathrm{m/s^2}$, multiplying the scale by 10 will convert the accelerometer data to $\mathrm{m/s^2}$, which was the only adjustment made to the acceleration data.

Finally, Fig. 11 shows the result of trajectory P1 from Fig. 6, after applying the process presented in Section 6.1. The result of the gravity vector and the magnitude of the field can be observed after applying the rotation defined by the quaternion. The absolute orientation obtained from fused data from a 3D accelerometer and magnetometer can be used in a variety of applications, including navigation, motion tracking, fall detection, virtual reality, and robotics. Using more than one sensor at a time for each measurement can help to improve the accuracy, robustness, and flexibility of the orientation measurement. As sensor technology continues to improve, the use of multiple sensors for orientation measurement will become even more common in a variety of devices and applications.

7.2. Geolocated data

To demonstrate the practical application of geopositioning, Fig. 12 depicts a map of the Campus Fraternidad at the Instituto Tecnológico Metropolitano, where the markers represent the magnitude of the magnetic field in microTeslas. Notably, a spatially-defined region on the eastern side of the campus exhibits blue-colored markers, which indicate a considerably low magnetic field intensity. It is worth noting that the data acquisition was performed on two separate days and subsequently superimposed to confirm the repeatability of the results.

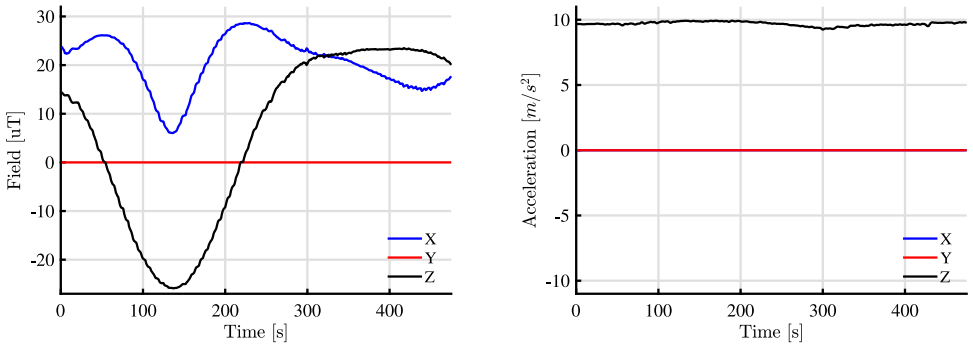

(a) X (b) Y

Fig. 11. Accelerometer data.

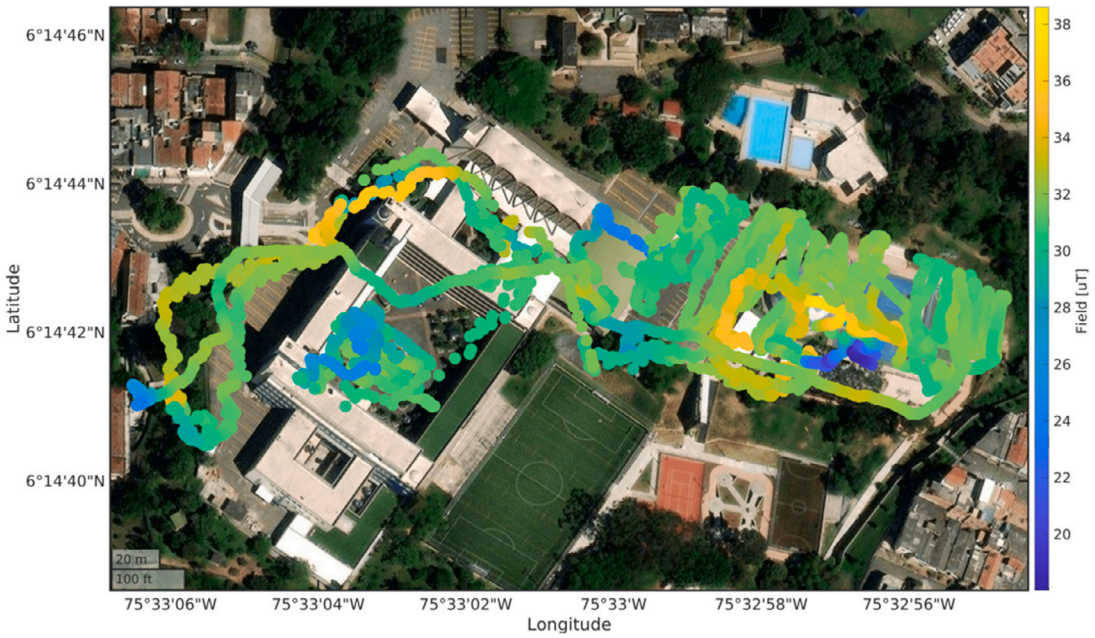

Fig. 12. Map of the Campus Fraternidad at the Instituto Tecnol'ogico Metropolitano, where the markers represent the magnitude of the magnetic field in microTeslas. (For interpretation of the references to color in this figure legend, the reader is referred to the web version of this article.)

Finally, in Fig. 13, another visualization method is presented that can be of great utility. In this method, the data points collected during the two Campus surveys are used, and interpolation is performed based on the magnetic field strength values, allowing for an estimation of the field strength at any point within the interpolated region. This visualization provides a clearer view of the low-field region on the eastern side.

8. Discussion and future work

In conclusion, the proposed system has the ability to generate maps of magnetic field strength in open spaces. These maps can be used to identify anomalous areas, which can be useful for various applications such as geology, mineral exploration, and environmental monitoring. By providing detailed information on changes in the magnetic field, the system has the potential to enhance our understanding of the Earth's magnetic field and its impact on our planet.

Open-access projects have the potential to democratize science and give access to local information. By making scientific knowledge and evidence freely accessible to all, these projects can help remove barriers to access and promote equity in scientific research.

In the future, the system will be further developed into software by creating tools that facilitate and analyze the interpretation of the data, making it easier for non-computer professionals to use and support their research areas. In many cases, manual processes are used to acquire scientific information, making the research process extremely complicated and time-consuming.

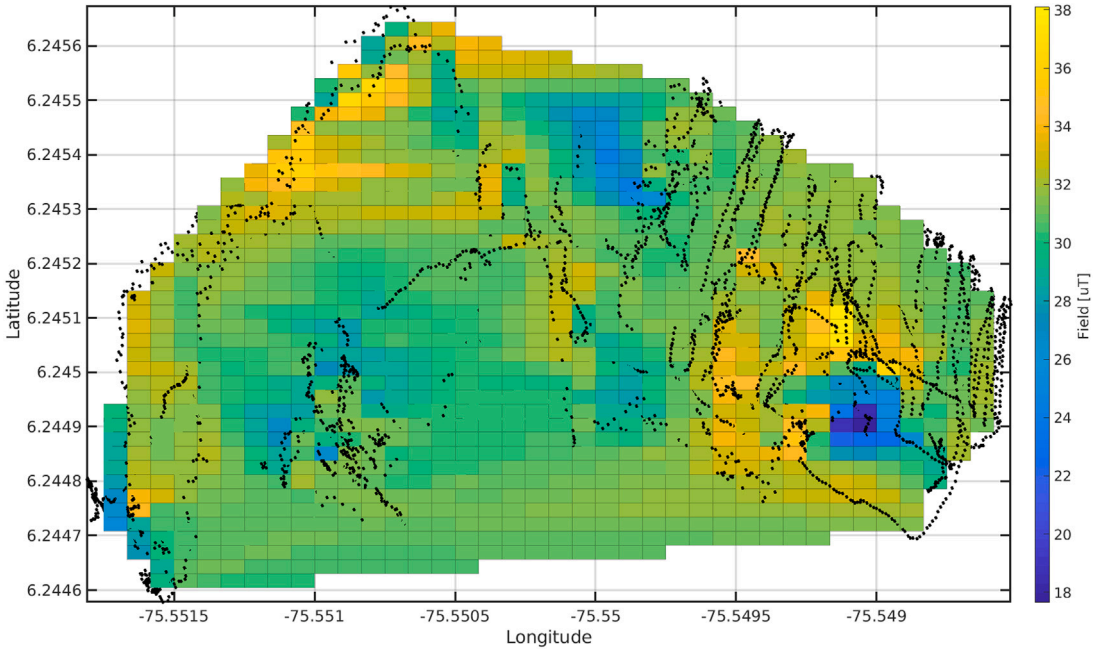

Fig. 13. Map of the magnetic field in microTeslas of The Campus Fraternidad at the Instituto Tecnol'ogico Metropolitano, with the interpolated markers.

Human and animal rights

No human or animal studies were conducted in this work.

Declaration of competing interest

The authors declare the following financial interests/personal relationships which may be considered as potential competing interests: The considerable sources of funding are related to the affiliation of the authors: Instituto Technológico Metropolitano, Medellín — Colombia. Institución Universitaria de Envigado, Medellín — Colombia.

Acknowledgments

This study were supported by the Sistemas de Control *y* Robótica (GSCR) Group COL0123701, at the Sistemas de Control *y* Robótica Laboratory, attached to the Instituto Tecnológico Metropolitano and the program "Propuesta para el fortalecimiento de tecnologías con potencial de transferencia", ITM-SAPIENCIA inter-administrative agreement. This work was supported in part by collaboration with REDTPI4.0 CYTED program.

References

[1] T. Nan, Y. Hui, M. Rinaldi, N.X. Sun, Self-biased 215 MHz magnetoelectric NEMS resonator for ultra-sensitive DC magnetic field detection, Sci. Rep. 3 (2013) 1–6, http://dx.doi.org/10.1038/srep01985.

[2] R. Gupta, R.K. Kotnala, A review on current status and mechanisms of room-temperature magnetoelectric coupling in multiferroics for device applications, J. Mater. Sci. 57 (27) (2022) 12710–12737, http://dx.doi.org/10.1007/s10853-022-07377-4.

[3] D. Ibáñez, E. García, J. Soret, J. Martos, Real-time condition monitoring system for electrode alignment in resistance welding electrodes, Sensors 22 (21) (2022) http://dx.doi.org/10.3390/s22218412.

[4] D. Murzin, D.J. Mapps, K. Levada, V. Belyaev, A. Omelyanchik, L. Panina, V. Rodionova, Ultrasensitive magnetic field sensors for biomedical applications, Sensors 20 (6) (2020) http://dx.doi.org/10.3390/s20061569.

[5] M. Zaeimbashi, M. Nasrollahpour, A. Khalifa, A. Romano, X. Liang, H. Chen, N. Sun, A. Matyushov, H. Lin, C. Dong, Z. Xu, A. Mittal, I. Martos-Repath, G. Jha, N. Mirchandani, D. Das, M. Onabajo, A. Shrivastava, S. Cash, N.X. Sun, Ultra-compact dual-band smart NEMS magnetoelectric antennas for simultaneous wireless energy harvesting and magnetic field sensing, Nature Commun. 12 (1) (2021) http://dx.doi.org/10.1038/s41467-021-23256-z.

[6] Y. Cong, C. Gu, T. Zhang, Y. Gao, Underwater robot sensing technology: A survey, Fund. Res. 1 (3) (2021) 337–345, http://dx.doi.org/10.1016/j.fmre.2021.03.002.

[7] J.L. Webb, J.D. Clement, L. Troise, S. Ahmadi, G.J. Johansen, A. Huck, U.L. Andersen, Nanotesla sensitivity magnetic field sensing using a compact diamond nitrogen-vacancy magnetometer, Appl. Phys. Lett. 114 (23) (2019) http://dx.doi.org/10.1063/1.5095241.

[8] J.E. Baader, S. Casalbuoni, E. Xfel, Pulsed wire magnetic field measurement system for short-period long undulators, in: Proceedings of IPAC2021, JACoW Publishing, 2021, pp. 2903–2906, http://dx.doi.org/10.18429/JACoW-IPAC2021-WEPAB126.

[9] S. Tumanski, Modern magnetic field sensors—A review, Organ 10 (1) (2013) 1–12, URL http://www.red.pe.org.pl/articles/2013/10/1.pdf.

[10] C. Becker, D. Karnaushenko, T. Kang, D.D. Karnaushenko, M. Faghih, A. Mirhajivarzaneh, O.G. Schmidt, Self-assembly of highly sensitive 3D magnetic field vector angular encoders, Sci. Adv. 5 (12) (2019) 1–11, http://dx.doi.org/10.1126/sciadv.aay7459.
[11] V. Vesterinen, S. Ruffieux, A. Kalaboukhov, H. Sipola, M. Kiviranta, D. Winkler, J.F. Schneiderman, J. Hassel, Magnetic field sensing with the kinetic inductance of a high- T c superconductor, AIP Adv. 9 (4) (2019) http://dx.doi.org/10.1063/1.5080798, arXiv:1810.12725.
[12] A. Poulose, O.S. Eyobu, D.S. Han, An indoor position-estimation algorithm using smartphone IMU sensor data, IEEE Access 7 (2019) 11165–11177, http://dx.doi.org/10.1109/ACCESS.2019.2891942.
[13] R. Yan, F. Zhang, H. Chen, A MEMS-based magnetometer calibration approach in AUV navigation system, in: OCEANS 2019 - Marseille, OCEANS Marseille 2019, 2019-June, IEEE, 2019, pp. 1–6, http://dx.doi.org/10.1109/OCEANSE.2019.8867368.
[14] H.J. Kim, K.C. Kwon, D.S. Shim, Fast algebraic calibration of MEMS tri-axis magnetometer for initial alignment using least square method, J. Electr. Eng. Technol. 15 (5) (2020) 2361–2372, http://dx.doi.org/10.1007/s42835-020-00516-4.
[15] F. Hu, Y. Wu, Y. Yu, J. Nie, W. Li, Q. Gao, An improved method for the magnetometer calibration based on ellipsoid fitting, in: Proceedings - 2019 12th International Congress on Image and Signal Processing, BioMedical Engineering and Informatics, CISP-BMEI 2019, (1) 2019, pp. 2–6, http://dx.doi.org/10.1109/CISP-BMEI48845.2019.8965821.
[16] PNIcorp, RM3100 real life applications, 2023, p. 1, URL https://www.pnicorp.com/our-products-at-work/.
[17] J.S. Bennett, B.E. Vyhnalek, H. Greenall, E.M. Bridge, F. Gotardo, S. Forstner, G.I. Harris, F.A. Miranda, W.P. Bowen, Precision magnetometers for aerospace applications: A review, Sensors 21 (16) (2021) 5568, http://dx.doi.org/10.3390/s21165568.
[18] J. Botero-Valencia, D. Marquez-Viloria, L. Castano-Londono, L. Morantes-Guzmán, A low-cost platform based on a robotic arm for parameters estimation of inertial measurement units, Measurement 110 (2017) 257–262, http://dx.doi.org/10.1016/j.measurement.2017.07.002.

J.S. Botero-Valencia is a Magister in Automation and Industrial Control, and Ph.D. in Engineering. He has experience in control systems and robotics, specifically in the Internet of Things (IoT) and mobile robotics. He currently works as a Professor in the Department of Mechatronics and Electromechanics of the Faculty of Engineering of the Instituto Tecnológico Metropolitano, and belongs to the Laboratory of Control Systems and Robotics.

Mateo Mejia-Herrera is a Mechatronic Engineer and M.Sc.(e) in Automation and Industrial Control of Instituto Tecnológico Metropolitano, Medellin, Colombia. He is member of the research group ‘‘Automática, Electrónica y Ciencias Computacionales’’ (classification A1) since 2018 with experience in artificial vision, embedded systems, IoT, and 3D printing for the development of low cost prototypes. He currently works as a Professor in the Department of Mechatronics and Electromechanics of the Faculty of Engineering of the Instituto Tecnológico Metropolitano, and belongs to the Laboratory of Control Systems and Robotics.

D. Betancur-Vásquez Mechatronic Engineer of the Metropolitan Technological Institute, and Magister in Automation and Industrial Control, with experience in control systems and robotics, specifically in mobile robotics, mechanical prototyping, data analysis and electronic development. He is currently a Professor in the engineering department in Institución Universitaria de Envigado and laboratory in the Control and Robotics Systems Laboratory of the Instituto Tecnológico Metropolitano.